







Ciliary propulsion and metachronal coordination in reef coral larvae

Rebecca N. Poon ¹, Timothy A. Westwood,² Hannah Laeverenz-Schlogelhofer ¹, Emelie Brodrick ¹, Jamie Craggs ^{3,2},
Eric E. Keaveny ¹, Gáspár Jékely,¹ and Kirsty Y. Wan ^{1,*}

¹Living Systems Institute, University of Exeter, Exeter EX4 4QD, United Kingdom

²Department of Mathematics, Imperial College London, London SW7 2AZ, United Kingdom

³Horniman Museum and Gardens, London SE23 3PQ, United Kingdom



(Received 19 September 2022; revised 12 July 2023; accepted 30 October 2023; published 11 December 2023)

Larval dispersal is critical to the survival of coral reefs. As the only motile stage of the reproductive cycle, coral larvae choose a suitable location to settle and mature into adult corals. Here, we present a detailed study of ciliary propulsion in the common stony reef coral *Acropora millepora*. Using high-speed, high-resolution imaging, particle image velocimetry, and electron microscopy, we reveal the arrangement of the densely packed cilia over the larval body surface, and their organization into diaplectic (transversely propagating) metachronal waves. We resolve the individual cilium's beat dynamics and compare the resulting flows with a computational model of a dense ciliary array, and evaluate the efficiency of flow pumping associated with diaplectic metachronism in different regimes.

DOI: [10.1103/PhysRevResearch.5.L042037](https://doi.org/10.1103/PhysRevResearch.5.L042037)

Ciliary motion is a distinctive and widespread method of propulsion across many aquatic species [1,2]. Many planktonic organisms have cilia either covering their whole body, or localized into rings or lobed structures called ciliary bands [3,4]. Unlike in cells with only a few cilia, such as sperm, or the biflagellate alga *Chlamydomonas* [5], arrays of beating cilia often exhibit sustained, long-range coordination of their beat phase, known as a metachronal wave (MCW), generating fluid flows whose global properties depend on the coordination patterns [6]. Thus, by organizing ciliary activity, these tiny organisms can feed, swim, avoid predators, and regulate their position in the water column [7,8].

Cilia are present in the larvae of many marine invertebrates. The larval stage is that unique and critical phase of an organism's life cycle that precedes or disguises its ultimate, mature form—hence the etymology of the term “larva” from the Latin for a ghost, demon, or mask [9]. The common reef-building coral *Acropora millepora*, which is a broadcast spawning coral, produces motile larvae [10] following a short period of pelagic development. These settle and mature into adult colonies (Fig. 1), within ~50 days [11]. A suitable choice of location is vital for postsettlement survival [12]. Larval swimming and settlement depends on a variety of external cues such as light and chemicals [13–15], although this behavior is little understood from either a biophysical or a signaling perspective. Swimming is achieved by the beating of multiple cilia, densely distributed over the entire body

surface. Although the primary role of these cilia is motility, they have also been shown to be useful in protecting larvae from suspended sediments [16].

Despite the obvious significance of coral larval motility for their survival to maturity, quantification of motility parameters or cilia behavior is lacking. In this Letter, we present a complete biophysical characterization of ciliary motility and propulsion in a coral larva. We perform experimental measurements across scales, from flows induced by a single larva, down to the dynamics of individual cilia. Combining high-speed imaging and micromanipulation, we also resolve the beating waveforms of cilia, and show that surface cilia exhibit diaplectic metachronal coordination. Finally, we compare these data with a computational model of a densely ciliated array, to rationalize the likely functional significance of this ciliary coordination strategy for motility and flow pumping efficacy.

Methods. *A. millepora* larvae were cultured *ex situ* [17,18]. Annual spawning occurred during the winter of 2020/21 and live embryos (3 days postfertilization) were transported directly from Horniman Museum and Gardens (London, U.K.) to an animal facility (University of Exeter, U.K.). Embryos were housed in artificial seawater containers inside incubators set to 27 °C. Larvae were fixed for scanning electron microscopy (SEM) in 2% glutaraldehyde at 4 days postfertilization, dehydrated in ethanol, and air dried in hexamethyldisilazane. After mounting on an aluminum sample pin with a carbon conductive tab, they were sputter coated with 10 nm gold/palladium. Images of the larvae and their ciliated ectodermal surface were taken with a field scanning electron microscope (Zeiss GeminiSEM 500, Carl Zeiss Corporation) using a 5 kV beam. For flow-field and particle image velocimetry (PIV) measurements, the fluid was seeded with 1- μm Fluoresbrite[®] multifluorescent microspheres at a volume fraction of $\approx 10^{-5}$ v/v. Videos were postprocessed

*k.y.wan2@exeter.ac.uk

Published by the American Physical Society under the terms of the Creative Commons Attribution 4.0 International license. Further distribution of this work must maintain attribution to the author(s) and the published article's title, journal citation, and DOI.

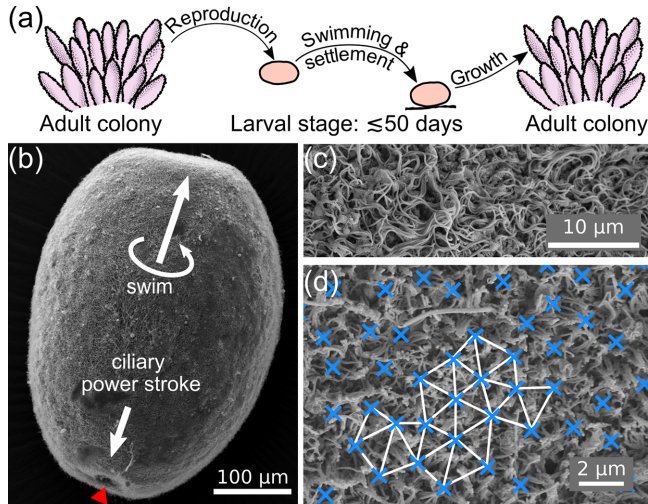


FIG. 1. (a) Key stages of the coral reproductive cycle: An adult colony releases egg/sperm bundles, which combine to produce motile larvae. These eventually settle and metamorphose into an adult polyp, beginning a new colony. Scanning electron micrographs of (b) a whole *A. millepora* larva (oral pore marked by a red arrowhead), (c) the densely ciliated surface, and (d) a quasi-hexagonal arrangement of the cilia basal bodies in a deciliated preparation. Cilia bases (blue \times) are surrounded by rings of microvilli.

using PIVlab [19]. Videos of individual free-swimming larvae in 500–600 μl droplets were captured at 80.5 fps using a Photometrics PRIME 95B camera mounted on a Nikon Ti2-U microscope, imaged with a $4\times$ objective (CFI Plan Fluor) in autofluorescence (CoolLED pE300-ultra SB). Single-larva micromanipulation experiments were conducted using TW-1200 borosilicate glass micropipettes pulled using a P-1000 Puller (Sutter Instruments). Pipettes were scored and broken off to give an outer diameter of $(100 \pm 10) \mu\text{m}$, and fire polished to give a rounded tip with inner diameter $(35 \pm 10) \mu\text{m}$. High-speed images (100–1000 fps) were captured using a Phantom V1212 camera mounted on a Leica DMi8 inverted microscope, using brightfield or differential interference contrast microscopy.

Experimental results. The larvae show a variety of body shapes, which can also change dynamically in time due to the animal’s developing musculature [20]. The basic shape is a prolate spheroid, with a slight narrowing and flattening at the oral pole. Larvae swim with the aboral pole facing forwards [Fig. 1(b)]. Typical larval dimensions are length $\sim(785 \pm 119) \mu\text{m}$, width $\sim(404 \pm 29) \mu\text{m}$, with aspect ratios $\alpha \sim 1.96 \pm 0.37$. Our SEM images show monociliated ectodermal cells, with each cilium surrounded by a ring of microvilli. The basal bodies show quasi-hexagonal order with lattice constant $a = (1.8 \pm 0.4) \mu\text{m}$ [Figs. 1(c) and 1(d)], so one larva has $\mathcal{O}(10^5)$ cilia. The length of the motile, body cilia is $L = (18 \pm 2) \mu\text{m}$. Here, $a/L = 0.1$, comparable to the densely ciliated *Paramecium*, where $a/L = 0.15$ [21].

We measured an average forward swimming speed of $(0.86 \pm 0.06) \text{mm s}^{-1}$, and an axial rotation frequency of $(0.23 \pm 0.09) \text{Hz}$ (data from $N = 4$ individuals). A full characterization of the free-swimming behavior will appear elsewhere [22]. Here, to estimate flow fields by PIV, we select

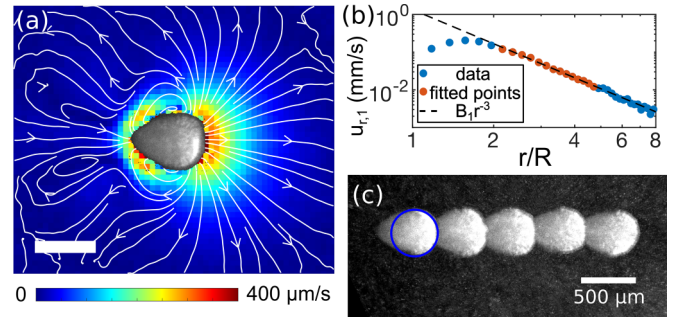


FIG. 2. The flow field and streamlines around a free-swimming coral larva (a). (Scale bar: 500 μm .) (b) The first radial Legendre coefficient for our data. Orange points were used to fit the strength B_1 of the source dipole moment, which decays as r^{-3} . Radial distance r is normalized by the effective squirmer radius R for plotting clarity (see text). (c) Silhouettes of the free-swimming larva at 0.5 s intervals. The blue circle shows the effective squirmer radius $R = 256 \mu\text{m}$.

portions of the larval trajectories with low curvature, where the larvae remain in the focal plane, in order to describe the basic, straight-swimming behavior. The flow fields were then shifted and rotated to place the larvae at the center, and swimming towards the right-hand side, of the frame. Azimuthally averaged flows were obtained by averaging over at least one body rotation period Fig. 2(a). (See Video 1 in the Supplemental Material [20] for further examples.)

The coral larvae have an average forward swimming speed of $U \sim 860 \mu\text{m s}^{-1}$, and an approximate radius of $\ell \sim 300 \mu\text{m}$. Thus, the Reynolds number for larval motion is $\text{Re} = \rho U \ell / \eta \sim 0.26$ (fluid density ρ and viscosity η), suggesting a minimal effect of fluid inertia.

Based on this and the high cilia density, we can model the swimmer as a “squirmer” [23,24]. Squirmer motion is obtained by specifying a velocity on some continuous, nondeforming surface and solving for the resulting fluid flow subject to the no-slip condition, as well as the conditions that the total force and torque are zero. For a densely ciliated organism, the surface corresponds to the envelope covering the cilia tips, and the prescribed velocity represents the ciliary beat dynamics.

Sufficiently close to the larva surface in the region where fluid inertia is negligible, the radial and tangential components, u_r and u_ϕ , respectively, for an azimuthally symmetric flow field (such as that around a spherical squirmer) in the laboratory frame can be expressed as

$$u_r(r, \phi) = \frac{2 B_1}{3 r^3} P_1 + \sum_{n=2}^{\infty} \left[\frac{A_n}{r^n} + \frac{B_n}{r^{n+2}} \right] P_n,$$

$$u_\phi(r, \phi) = \frac{1 B_1}{3 r^3} V_1 + \sum_{n=2}^{\infty} \left[\frac{n-2}{2} \frac{A_n}{r^n} + \frac{n}{2} \frac{B_n}{r^{n+2}} \right] V_n,$$

where ϕ is the polar angle, P_n are the Legendre polynomials of $\cos \phi$, and

$$V_n = \frac{2 \sin \phi}{n(n+1)} P'_n(\cos \phi),$$

where the prime $'$ denotes the derivative with respect to $\cos \phi$ [23–25]. The coefficients A_n and B_n give the strength of the n th-order force and source multipoles, respectively, where B_1

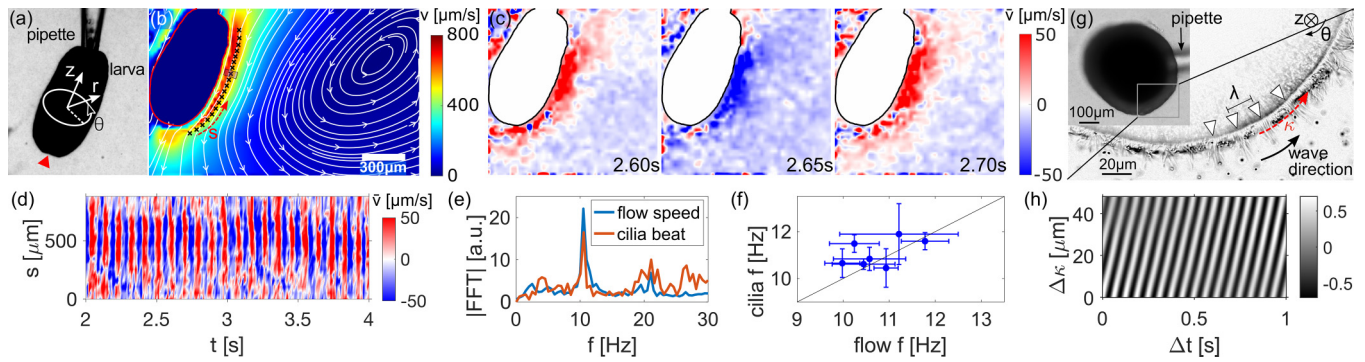


FIG. 3. (a) PIV performed on single coral larvae tethered by gentle micropipette suction at the aboral end. (b) An example time-averaged flow field. (Streamlines shown in white. The color bar indicates flow speed, and scale bar $300\ \mu\text{m}$.) (c) Three snapshots of the mean-subtracted flow speed \bar{v} spaced at $50\ \text{ms}$. (d) Space-time kymograph of the near-field flow \bar{v} along the side of the larval body. Fourier transforms of the flow speed and the cilia beat peak at the same frequency (e) for the pictured larva, and (f) for the population ($N = 7$). (g) Observation of a larva tethered in “top-down” configuration (\mathbf{e}_z into the page) reveals metachronal wave crests. (h) Autocorrelation of cilia intensity along the ciliary band.

is the source dipole (related to the prescribed surface velocity). The force monopole term $A_1 = 0$ for force-free swimmers. Our swimmer swims in the z direction with its center at the origin of the coordinate system.

For a spherical squirmer with surface velocities corresponding to source- and force-dipole flows, the swimming speed is given by $U/U_0 = 1 - (3\beta/20)\text{Re} + \mathcal{O}(\text{Re}^2)$, [26] where β is the ratio of the strengths of the force and source coefficients, and $U_0 = 2B_1/3R^3$ is the Stokes flow swimming speed [25].

We compute B_1 by evaluating $u_{r,n}(r) = \frac{2n+1}{2} \int_0^\pi u_r P_n(\cos\phi) \sin\phi d\phi$ for $n = 1$, which gives $2B_1/3r^3$. For the larva in Fig. 2(a), $u_{r,1}(r)$ is plotted in Fig. 2(b). We observe the expected r^{-3} decay. Fitting the decay in a region close to the larva gives the source-dipole strength $B_1 = 2.2 \times 10^{10}\ \mu\text{m}^4\ \text{s}^{-1}$. By fitting $u_{r,2}$ for our flows, we estimate $\beta = -0.13$ for this larva (see Supplemental Material [20] for details). For the measured larva speed $U = 890\ \mu\text{m}\ \text{s}^{-1}$ and the above values of B_1 , β , and Re , rearranging the previous expression for U gives a swimmer radius $R = 256\ \mu\text{m}$. We note that $\mathcal{O}(\text{Re})$ correction produces only a 0.5% difference in the speed from U_0 . Thus, to a first approximation the larva is a spherical squirmer with an effective radius of $\sim 256\ \mu\text{m}$. Although the larva is teardrop shaped, the fitted circle shows a good match to the size of the “head” [Fig. 2(c)].

To resolve the dynamics of the ciliated surface in detail, we tethered larvae to micropipettes in a variety of orientations. To specify these orientations, we now refer to a cylindrical coordinate system with \mathbf{e}_z pointing in the larval swimming direction, and the azimuthal angle θ defined in a right-handed sense. First, we tethered the larvae *sideways*, with \mathbf{e}_z in the image plane [Fig. 3(a)]. The time-averaged flow field around a *sideways* larva is shown in Fig. 3(b). The maximum near-field tangential flow speed is similar to the maximum tangential flows measured in the comoving frame of the free-swimming larva, indicating that the native ciliary behavior was not adversely affected by the pipette. The presence of vortices in the flow is likely due to confinement in the direction normal to the image plane [27].

Using time-resolved flow fields as a proxy for the ciliary beat phase, we compute fluctuations around the mean flow

speed, $\bar{v}(\mathbf{x}, t) = v(\mathbf{x}, t) - \langle v(\mathbf{x}) \rangle_t$. In the sideways orientation, \bar{v} shows a periodic “blinking” behavior [Fig. 3(c)]. The near-field flow speed is plotted as a function of time and arclength along the larva in Fig. 3(d). The blinking appears as vertical lines on the kymograph, indicating that the cilia beat *in phase* along the aboral-oral axis. This is in contrast to PIV data from the model squirmer *V. carteri*, a spherical alga that shows alternating patches of high and low flow speed along the beat direction due to a MCW that propagates *in* the beat direction [28]. To confirm that the flow periodicity is due to ciliary beating, we compare in the same video the Fourier transform of the flow speed with that of pixel intensity fluctuations at the surface—a proxy for cilia beating. Both show peaks at the same frequency of 10.5 Hz [Fig. 3(e)]. Cilia beating matches the flow oscillation frequencies in seven different larvae [Fig. 3(f)], for videos lasting $\gtrsim 50$ beat periods.

This implies that a diaplectic MCW with vertical wave crests is propagating in either the $+\mathbf{e}_\theta$ (*dexioplectic*, 90° anticlockwise from the power stroke) or $-\mathbf{e}_\theta$ direction (*laeoplectic*, 90° clockwise from the power stroke) [6]. To confirm the existence and direction of such a wave, we imaged the larvae in a *top-down* state [Fig. 3(g), Video 2 in Supplemental Material]. In this view, ciliary metachrony is clearly visible, and the wave propagates in the $-\mathbf{e}_\theta$ direction. The two-dimensional (time-space) autocorrelation of image intensity along the ciliary array as a function of time is used to estimate MCW parameters [29] [Fig. 3(h)]. Wavecrests appear as diagonal lines, whose spacing in κ and t give the wavelength and period respectively [Fig. 3(h)]. The wave was laeoplectic in all specimens where the wave direction could be deduced ($N = 6$). The cilia beat with frequency $(11.1 \pm 0.6)\ \text{Hz}$, and the MC wavelength is $(19 \pm 4)\ \mu\text{m}$.

Computational results. Thus, the cilia are coordinated metachronally along the surface of the coral larva body in the direction shown in Fig. 4(a). To reconcile the measured flow features with this putative ciliary coordination pattern, we developed a numerical simulation. Since the cilia are very short compared to the size of the larva (20–30 times), we approximate the curved ectoderm locally as a planar no-slip surface. A dense array of 1033 cilia of length L were arranged in a quasihexagonal lattice with spacing $\Delta_\theta = 0.1L$ in the

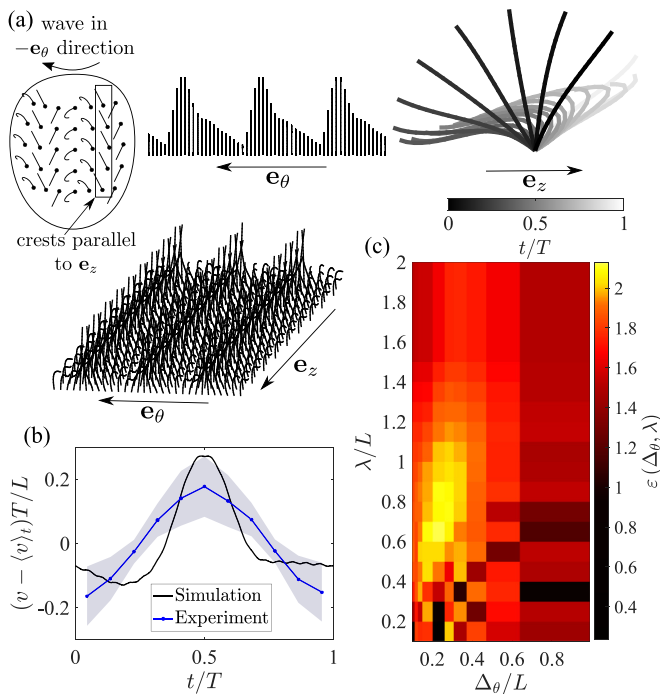


FIG. 4. (a) Simulation of an array of model cilia, with top-down view of the array and the model cilia waveforms over one cycle. Inset: Laeoplectic MCW on the larva (cilia not to scale). (b) Phase-dependent, mean-subtracted flow speed sampled in a box above the array in the simulations (black curve) compared with experiments (blue curve) ($N = 7$, average over multiple beat cycles; shaded region: standard deviation). (c) The pumping efficiency of arrays of laeoplectically coordinated cilia for different wavelengths λ and spacings Δ_θ .

direction orthogonal to the beat plane, and $\Delta_z = 1.12L$ in the beat direction (the minimum allowable separation such that neighboring cilia do not intersect). For each model cilium, its dynamics were prescribed according to high-speed tracking data (Video 3 in Supplemental Material), and beating was assumed to be largely planar. Manually traced ciliary waveforms were simplified by fitting to a low-order polynomial in space and a four-term Fourier series in time to yield the trace shown in Fig. 4(a), inset. Each cilium is discretized into $M = 20$ segments. For Stokes flow (a reasonable assumption since $\text{Re} \sim 0.06$ for the cilia), the cilium segment velocities \mathbf{V} and forces \mathbf{F} are linearly related via the dense mobility matrix \mathcal{M} . The resulting system is solved numerically using the generalized minimum residual (GMRES) method [20,30].

At a height of $\sim 5L/3$ above the no-slip boundary, and midway along the larval body, we evaluated \bar{v} induced by the computational array when the cilia are coordinated in a laeoplectic wave with wavelength $\lambda = L$, and compared this to the PIV-sampled flow data [Fig. 4(b)]. The simulations reproduced the periodic blinking in Fig. 3(b), where T is the beat period of the cilia. The quantitative agreement between the phase-dependent oscillatory flow profiles could be increased if technical limitations can be overcome (the inability of PIV to resolve near-field flows, difficulty of inferring 3D motion

from 2D images), and if the simulation can be made more realistic.

Finally, we explore the consequences of varying the wavelength λ of the laeoplectic wave and the wave-parallel cilia spacing Δ_θ on the dimensionless pumping efficiency $\varepsilon(\Delta_\theta, \lambda) = \eta \langle Q(\Delta_\theta, \lambda, t) \rangle_t^2 / (L^3 \langle \mathcal{R}(\Delta_\theta, \lambda, t) \rangle_t)$ of the cilia array, where Q is the total volume flow rate above the no-slip surface, $\mathcal{R} = \mathbf{V}^\top \mathbf{F}$ is the total power exerted on the fluid by the cilia, and $\langle \cdot \rangle_t$ denotes a time average [20]. The size of the array is kept fixed with lengths $8.9L$ and $19.04L$ in the θ and z directions, respectively, so the total number of cilia varies with spacing Δ_θ . The results in Fig. 4(c) reveal that the regime of high cilia density and wavelength $\lambda \sim L$ observed in the experiments corresponds to a high pumping efficiency. The efficiency maximum arises due to the ratio between the flow rate and viscous dissipation, which at low spacings individually increases (see Supplemental Material [20]).

Concluding remarks. Reef-building corals, including *Acropora* species, have huge ecological importance yet have proved impossible to culture under laboratory conditions, until recently [18]. Here, we have presented a biophysical study of cilia motility and coordination in a coral larva. Our multiscale approach spans individual cilium dynamics, their collective coordination, and cilia-induced flows around whole larvae. We found that the density of cilia in the ectoderm is high, allowing comparisons with a low-Re squirmer [23,24]. For larvae with aspect ratio close to unity, the free-swimming speeds are well described by that of spherical squirmer whose (effective) radius (obtained by our flow-field matching procedure) is comparable to the size of the larva. This is in spite of the deviation of larval morphology from perfect spheres, and further breaking of azimuthal symmetry by both cilia orientation and coordination.

The larvae rotate slowly about the aboral-oral axis while swimming. This may arise from slightly nonplanar ciliary beating, as seen in *Chlamydomonas* [5]. Here, we neglected azimuthal asymmetries by averaging free-swimming flows over multiple rotation periods, justified since the period of cilia beating (~ 0.1 s) is much smaller than that of body rotation (~ 5 s). We can naturally extend the spherical squirmer model to include azimuthal asymmetry [31], or more realistic spheroidal or rod-shaped larval morphologies [25], thereby coupling single-cilium dynamics with whole-larva propulsion [22].

We also make detailed observations of MCWs in a coral larva. By imaging body-fixed specimens in multiple orientations, we deduced that the wave is diaplectic (particularly, laeoplectic). This sense of MCWs should be compared with other cnidarians. Diaplectic waves have been described anecdotally in diverse invertebrate larvae [6,32], but in most other organisms where MCWs have been unambiguously characterized they are either symplectic [6,33], or antiplectic [34,35]. Generally, metachronism is expected in ensembles of cilia due to hydrodynamic interactions [36–38], but the wave direction remains highly system dependent and ultimately unexplained in living organisms. Insights from idealized scenarios, both simulated and artificial, emphasize the importance of the cilia beat pattern, organization, and boundary conditions [30,39–42]. Ciliary coordination could even be influenced by mucus, as shown in human bronchial epithe-

lia [43]. The larvae of the coral *Caryophyllia smithii* trail mucus strings from the oral pore to facilitate feeding [44]. Although it is not known whether *A. millepora* larvae are similar feeders, we observed “mucus trails” behind the swimming larvae. Mucus secretion [16] hinders our ability to perform near-field PIV [and could contribute to the two “lobes” in Fig. 2(a)].

From protists to humans, the patterning of cilia undergoes precise developmental control [29,45]. Diaplectic metachronism could be a key evolutionary driver for ciliary placement and basal-body orientation. Steric interactions will promote in-phase synchronization in the stroke direction, as interciliary spacing is so small ($0.1L$); in the transverse direction, however, phase shifts help prevent collisions between closely packed beating cilia [46]. Here, we simulated a dense ciliary array using beat patterns reconstructed from data, revealing the functional consequences of diaplectic MCWs for fluid

pumping. In the high cilia density limit, efficiency is very high at a wavelength comparable to the cilium length (as observed). However, to answer the question of how diaplectic waves actually emerge in the coral ectoderm, more experiments and modeling are needed.

Acknowledgments. This work was funded by the Human Frontier Science Programme Grant No. RGP0033/2020 (G.J.), an EPSRC Doctoral Prize Fellowship (EP/T51780X/1) (T.A.W.), and the European Research Council under the European Union’s Horizon 2020 research and innovation programme Grant No. 853560 EvoMotion (K.Y.W.). To induce ex situ coral spawning, reagents and aquarium filtration equipment were provided by Triton Applied Reef Biosciences and EcoTech Marine (J.C.). We acknowledge support from the Wolfson Bioimaging facility at the University of Bristol.

-
- [1] D. R. Mitchell, Evolution of cilia, *Cold Spring Harb. Perspect. Biol.* **9**, a028290 (2017).
- [2] K. Y. Wan and G. Jékely, On the unity and diversity of cilia, *Philos. Trans. R. Soc. B* **375**, 20190148 (2020).
- [3] C. Nielsen, Structure and function of metazoan ciliary bands and their phylogenetic significance, *Acta Zool.* **68**, 205 (1987).
- [4] W. Gilpin, V. N. Prakash, and M. Prakash, Vortex arrays and ciliary tangles underlie the feedingswimming trade-off in starfish larvae, *Nat. Phys.* **13**, 380 (2017).
- [5] D. Cortese and K. Y. Wan, Control of helical navigation by three-dimensional flagellar beating, *Phys. Rev. Lett.* **126**, 088003 (2021).
- [6] E. W. Knight-Jones, Relations between metachronism and the direction of ciliary beat in metazoa, *J. Micro. Sci.* **s3-95**, 503 (1954).
- [7] L. A. Bezares-Calderón, J. Berger, S. Jasek, C. Veraszto, S. Mendes, M. Gühmann, R. Almeda, R. Shahidi, and G. Jékely, Neural circuitry of a polycystin-mediated hydrodynamic startle response for predator avoidance, *eLife* **7**, e36262 (2018).
- [8] O. H. Shapiro, V. I. Fernandez, M. Garren, J. S. Guasto, F. P. Debaillon-Vesque, E. Kramarsky-Winter, A. Vardi, and R. Stocker, Vortical ciliary flows actively enhance mass transport in reef corals, *Proc. Natl. Acad. Sci. USA* **111**, 13391 (2014).
- [9] C. Linnaeus, *Systema naturae per regna tria naturae, secundum classes, ordines, genera, species, cum characteribus & differentiis. Tomus II. Editio duodecima, reformata* (Homiae, Stockholm, Laurentii Salvii, 1767).
- [10] P. L. Harrison, R. C. Babcock, G. D. Bull, J. K. Oliver, C. C. Wallace, and B. L. Willis, Mass spawning in tropical reef corals, *Science* **223**, 1186 (1984).
- [11] A. Nishikawa and K. Sakai, Settlement-competency period of planulae and genetic differentiation of the scleractinian coral *Acropora digitifera*, *Zool. Sci.* **22**, 391 (2005).
- [12] L. Harrington, K. Fabricius, G. De’Ath, and A. Negri, Recognition and selection of settlement substrata determine post-settlement survival in corals, *Ecology* **85**, 3428 (2004).
- [13] M. E. Strader, S. W. Davies, and M. V. Matz, Differential responses of coral larvae to the colour of ambient light guide them to suitable settlement microhabitat, *R. Soc. Open Sci.* **2**, 150358 (2015).
- [14] Y. Sakai, K. Kato, H. Koyama, A. Kuba, H. Takahashi, T. Fujimori, M. Hatta, A. P. Negri, A. H. Baird, and N. Ueno, A step-down photophobic response in coral larvae: implications for the light-dependent distribution of the common reef coral, *Acropora tenuis*, *Sci. Rep.* **10**, 17680 (2020).
- [15] H. Jorissen, P. E. Galand, I. Bonnard, S. Meiling, D. Raviglione, A.-L. Meistertzheim, L. Hédoquin, B. Banaigs, C. E. Payri, and M. M. Nugues, Coral larval settlement preferences linked to crustose coralline algae with distinct chemical and microbial signatures, *Sci. Rep.* **11**, 14610 (2021).
- [16] G. F. Ricardo, R. J. Jones, P. L. Clode, and A. P. Negri, Mucous secretion and cilia beating defend developing coral larvae from suspended sediments, *PLoS One* **11**, e0162743 (2016).
- [17] J. Craggs, J. R. Guest, M. Davis, J. Simmons, E. Dashti, and M. Sweet, Inducing broadcast coral spawning ex situ: Closed system mesocosm design and husbandry protocol, *Ecol. Evol.* **7**, 11066 (2017).
- [18] J. Craggs, J. Guest, M. Davis, and M. Sweet, Completing the life cycle of a broadcast spawning coral in a closed mesocosm, *Invertebr. Reprod. Dev.* **64**, 244 (2020).
- [19] W. Thielicke and E. Stamhuis, PIVLAB—towards user-friendly, affordable and accurate digital particle image velocimetry in matlab, *J. Open Res. Softw.* **2**, e30 (2014).
- [20] See Supplemental Material at <http://link.aps.org/supplemental/10.1103/PhysRevResearch.5.L042037> for additional information, which includes Refs. [47–54].
- [21] M. Kreutz, T. Stoeck, and W. Foissner, Morphological and molecular characterization of *Paramecium* (*Viridoparamecium* nov. subgen.) *chlorelligerum* Kahl, 1935 (Ciliophora), *J. Eukaryot. Microbiol.* **59**, 548 (2012).
- [22] H. Laeverenz Schlogelhofer *et al.*, Morphology and hydrodynamics of freely-swimming planula larvae (unpublished).
- [23] M. J. Lighthill, On the squirming motion of nearly spherical deformable bodies through liquids at very small Reynolds numbers, *Commun. Pure Appl. Math.* **5**, 109 (1952).
- [24] J. R. Blake, A spherical envelope approach to ciliary propulsion, *J. Fluid Mech.* **46**, 199 (1971).

- [25] A. W. Zantop and H. Stark, Squirmer rods as elongated microswimmers: flow fields and confinement, *Soft Matter* **16**, 6400 (2020).
- [26] N. G. Chisholm, D. Legendre, E. Lauga, and A. S. Khair, A squirmer across Reynolds numbers, *J. Fluid Mech.* **796**, 233 (2016).
- [27] R. E. Pepper, M. Roper, S. Ryu, P. Matsudaira, and H. A. Stone, Nearby boundaries create eddies near microscopic filter feeders, *J. R. Soc., Interface* **7**, 851 (2010).
- [28] D. R. Brumley, M. Polin, T. J. Pedley, and R. E. Goldstein, Metachronal waves in the flagellar beating of *Volvox* and their hydrodynamic origin, *J. R. Soc., Interface* **12**, 20141358 (2015).
- [29] K. Y. Wan, S. K. Hürlimann, A. M. Fenix, R. M. McGillivray, T. Makushok, E. Burns, J. Y. Sheung, and W. F. Marshall, Reorganisation of complex ciliary flows around regenerating *Stentor coeruleus*, *Philos. Trans. R. Soc., B* **375**, 20190167 (2019).
- [30] T. A. Westwood and E. E. Keaveny, Coordinated motion of active filaments on spherical surfaces, *Phys. Rev. Fluids* **6**, L121101 (2021).
- [31] O. S. Pak and E. Lauga, Generalized squirming motion of a sphere, *J. Eng. Math.* **88**, 1 (2014).
- [32] M. Marinković, J. Berger, and G. Jékely, Neuronal coordination of motile cilia in locomotion and feeding, *Philos. Trans. R. Soc., B* **375**, 20190165 (2020).
- [33] D. R. Brumley, M. Polin, T. J. Pedley, and R. E. Goldstein, Hydrodynamic synchronization and metachronal waves on the surface of the colonial alga *Volvox carteri*, *Phys. Rev. Lett.* **109**, 268102 (2012).
- [34] H. Machemer, Ciliary activity and the origin of metachrony in *Paramecium*: Effects of increased viscosity, *J. Exp. Biol.* **57**, 239 (1972).
- [35] S. L. Tamm, Mechanisms of ciliary coordination in ctenophores, *J. Exp. Biol.* **59**, 231 (1973).
- [36] G. R. Ramirez-San Juan, A. J. T. M. Mathijssen, M. He, L. Jan, W. Marshall, and M. Prakash, Multi-scale spatial heterogeneity enhances particle clearance in airway ciliary arrays, *Nat. Phys.* **16**, 958 (2020).
- [37] D. R. Brumley, K. Y. Wan, M. Polin, and R. E. Goldstein, Flagellar synchronization through direct hydrodynamic interactions, *eLife* **3**, e02750 (2014).
- [38] N. Pellicciotta, D. Das, J. Kotar, M. Faucourt, N. Spassky, E. Lauga, and P. Cicuta, Cilia density and flow velocity affect alignment of motile cilia from brain cells, *J. Exp. Biol.* **223**, jeb229310 (2020).
- [39] F. Meng, R. R. Bennett, N. Uchida, and R. Golestanian, Conditions for metachronal coordination in arrays of model cilia, *Proc. Natl. Acad. Sci. USA* **118**, e2102828118 (2021).
- [40] X. Dong, G. Z. Lum, W. Hu, R. Zhang, Z. Ren, P. R. Onck, and M. Sitti, Bioinspired cilia arrays with programmable non-reciprocal motion and metachronal coordination, *Sci. Adv.* **6**, eabc9323 (2020).
- [41] J. Elgeti and G. Gompper, Emergence of metachronal waves in cilia arrays, *Proc. Natl. Acad. Sci. USA* **110**, 4470 (2013).
- [42] H. Guo, J. Nawroth, Y. Ding, and E. Kansa, Cilia beating patterns are not hydrodynamically optimal, *Phys. Fluids* **26**, 091901 (2014).
- [43] O. Mesdjian, C. Wang, S. Gsell, U. D’Ortona, J. Favier, A. Viallat, and E. Loiseau, Longitudinal to transverse metachronal wave transitions in an *in vitro* model of ciliated bronchial epithelium, *Phys. Rev. Lett.* **129**, 038101 (2022).
- [44] P. Tranter, D. Nicholson, and D. Kinchington, A description of spawning and post-gastrula development of the cool temperate coral, *Caryophyllia smithii*, *J. Mar. Biolog. Assoc.* **62**, 845 (1982).
- [45] N. Spassky and A. Meunier, The development and functions of multiciliated epithelia, *Nat. Rev. Mol.* **18**, 423 (2017).
- [46] C. Ringers, S. Bialonski, M. Ege, A. Solovov, J. N. Hansen, I. Jeong, B. M. Friedrich, and N. Jurisch-Yaksi, Novel analytical tools reveal that local synchronization of cilia coincides with tissue-scale metachronal waves in zebrafish multiciliated epithelia, *eLife* **12**, e77701 (2023).
- [47] J. R. Blake, A note on the image system for a stokeslet in a no-slip boundary, *Math. Proc. Cambridge Philos. Soc.* **70**, 303 (1971).
- [48] Y. Saad and M. Schultz, GMRES: A generalized minimal residual algorithm for solving nonsymmetric linear systems, *SIAM J. Sci. Comput.* **7**, 856 (1986).
- [49] J. Nickolls, I. Buck, M. Garland, and K. Skadron, Scalable parallel programming with CUDA, *Queue* **6**, 40 (2008).
- [50] J. W. Swan and J. F. Brady, Simulation of hydrodynamically interacting particles near a no-slip boundary, *Phys. Fluids* **19**, 113306 (2007).
- [51] J. Blake, A model for the micro-structure in ciliated organisms, *J. Fluid Mech.* **55**, 1 (1972).
- [52] N. Nakanishi, D. Yuan, D. K. Jacobs, and V. Hartenstein, Early development, pattern, and reorganization of the planula nervous system in *Aurelia* (cnidaria, scyphozoa), *Dev. Genes Evol.* **218**, 511 (2008).
- [53] Y. Ding, J. C. Nawroth, M. J. McFall-Ngai, and E. Kansa, Mixing and transport by ciliary carpets: A numerical study, *J. Fluid Mech.* **743**, 124 (2014).
- [54] D. Smith, J. Blake, and E. Gaffney, Fluid mechanics of nodal flow due to embryonic primary cilia, *J. R. Soc., Interface* **5**, 567 (2008).